

## THE EXTREME SMALL SCALES: DO SATELLITE GALAXIES TRACE DARK MATTER?

DOUGLAS F. WATSON<sup>1</sup>, ANDREAS A. BERLIND<sup>1,2</sup>, CAMERON K. MCBRIDE<sup>1</sup>, DAVID W. HOGG<sup>3,4</sup>, TAO JIANG<sup>3</sup>

*Draft version December 3, 2024*

### ABSTRACT

We investigate the radial distribution of galaxies within their host dark matter halos by modeling their small-scale clustering, as measured in the Sloan Digital Sky Survey. Specifically, we model the Jiang et al. (2011) measurements of the galaxy two-point correlation function down to very small projected separations ( $10 \leq r \leq 400h^{-1}\text{kpc}$ ), in a wide range of luminosity threshold samples (absolute  $r$ -band magnitudes of  $-18$  up to  $-23$ ). We use a halo occupation distribution (HOD) framework with free parameters that specify both the number and spatial distribution of galaxies within their host dark matter halos. We assume that the first galaxy in each halo lives at the halo center and that additional satellite galaxies follow a radial density profile similar to the dark matter Navarro-Frenk-White (NFW) profile, except that the concentration and inner slope are allowed to vary. We find that in low luminosity samples ( $M_r < -19.5$  and lower), satellite galaxies have radial profiles that are consistent with NFW.  $M_r < -20$  and brighter satellite galaxies have radial profiles with significantly steeper inner slopes than NFW (we find inner logarithmic slopes ranging from  $-1.6$  to  $-2.1$ , as opposed to  $-1$  for NFW). We define a useful metric of concentration,  $M_{1/10}$ , which is the fraction of satellite galaxies (or mass) that are enclosed within one tenth of the virial radius of a halo. We find that  $M_{1/10}$  for low luminosity satellite galaxies agrees with NFW, whereas for luminous galaxies it is  $2.5 - 4$  times higher, demonstrating that these galaxies are substantially more centrally concentrated within their dark matter halos than the dark matter itself. Our results therefore suggest that the processes that govern the spatial distribution of galaxies, once they have merged into larger halos, must be luminosity dependent, such that luminous galaxies become poor tracers of the underlying dark matter.

*Subject headings:* cosmology: theory — galaxies: fundamental parameters — large-scale structure of universe — methods: statistical — surveys

### 1. INTRODUCTION

Determining the relationship between the spatial distributions of galaxies and dark matter remains one of the central problems of theoretical and observational cosmology. The radial distribution of galaxies within their host dark matter halos dictates how galaxies cluster on scales smaller than the virial radii of the largest dark matter halos ( $\lesssim 1h^{-1}\text{Mpc}$ ). Therefore, the measured galaxy correlation function itself is a powerful tool for shedding light on how galaxies trace the underlying dark matter within halos.

The halo occupation distribution (HOD) framework has been established as a robust method for modeling galaxy clustering by simply characterizing the biased relationship between galaxies and mass (see, e.g., Peacock & Smith 2000; Scoccimarro et al. 2001; Berlind & Weinberg 2002; Cooray & Sheth 2002; Zheng et al. 2005). The HOD describes this relation by specifying the probability distribution  $P(N|M)$  that a halo of mass  $M$  contains  $N$  galaxies, along with a prescription for the spatial distribution of galaxies within halos. For this latter component, it is typically assumed that a single ‘central’ galaxy lives at the center of each halo, with additional ‘satellite’ galaxies tracing

the dominant dark matter component. This assumption has been used successfully to model galaxy clustering on scales larger than  $r \sim 100h^{-1}\text{kpc}$  (e.g., Zehavi et al. 2004, 2005b, 2010; Zheng et al. 2007, 2009). However, Watson et al. (2010) showed that this assumption does not work to explain the smaller-scale clustering of luminous red galaxies (LRGs) in the Sloan Digital Sky Survey (SDSS; York et al. 2000). In order to achieve a good fit to the clustering of LRGs on scales smaller than  $\sim 100h^{-1}\text{kpc}$  (measured by Masjedi et al. 2006), they found that the radial profile of satellite LRGs must have a much steeper inner slope compared to the Navarro-Frenk-White (NFW; Navarro et al. 1997) dark matter profile. Watson et al. (2010) concluded that the distribution of satellite LRGs within halos is better described by an isothermal distribution.

Recently, Jiang et al. (2011) measured the projected two-point correlation function  $w_p(r_p)$  for several luminosity samples from the SDSS, extending the measurements done by Zehavi et al. (2010) on intermediate scales ( $\sim 0.1 - 40h^{-1}\text{Mpc}$ ) down to extremely small galaxy-galaxy separations ( $0.01 - 7h^{-1}\text{Mpc}$ ). Our motivation for this paper is to model the innermost data points ( $0.01 - 0.4h^{-1}\text{Mpc}$ ) in the same vein as Watson et al. (2010, hereafter W10) to see if there is a luminosity dependence of the radial profile of satellite galaxies.

The paper is laid out as follows. In §2, we review the Jiang et al. (2011, hereafter J11) measurements. In §3, we discuss our modeling method in the following manner: in §3.1 we provide an overview of the general technique used to model the small-scale correlation function; in §3.2

<sup>1</sup> Department of Physics and Astronomy, Vanderbilt University, 1807 Station B, Nashville, TN 37235

<sup>2</sup> Alfred P. Sloan Fellow

<sup>3</sup> Center for Cosmology and Particle Physics, Department of Physics, New York University, New York, NY, 10003

<sup>4</sup> Max-Planck-Institut für Astronomie, Königstuhl 17, D-69117 Heidelberg, Germany

we revisit the W10 four-parameter PNM model that allows the the probability distribution  $P(N|M)$  to vary, and the five-parameter PNMCG model that also allows the radial distribution of galaxies within halos to vary. We present our results in §4. Finally, we summarize and discuss the implications of our results in §5. Throughout the paper, we assume a  $\Lambda$ CDM cosmology with  $\Omega_m = 0.25$ ,  $\Omega_\Lambda = 0.75$ ,  $\Omega_b = 0.04$ ,  $h_0 = 0.7$ ,  $\sigma_8 = 0.8$ ,  $n_s = 1.0$ .

## 2. DATA

J11 measured the projected two-point correlation function down to very small scales ( $0.01 < r < 7h^{-1}\text{Mpc}$ ) for a large range of galaxy luminosity threshold samples. Both spectroscopic and imaging samples were used for computing  $w_p(r_p)$ . The imaging sample consists of  $\sim 10^8$  galaxies drawn from the SDSS imaging catalog. The spectroscopic sample is produced from the NYU VAGC (Blanton et al. 2005) V7.2 data (Abazajian et al. 2009) and contains  $8.6 \times 10^5$  SDSS Main Sample galaxies (Strauss et al. 2002),  $5 \times 10^5$  of which are in the redshift range  $0.03 < z < 0.15$ .

Measuring  $w_p(r_p)$  on very small scales is a non-trivial task. The SDSS spectroscopic sample suffers from incompleteness due to the physical size of the fiber-optic cables, which impede the ability to take spectra of two galaxies closer than  $55''$  on the sky. These “fiber collisions” thus result in a minimum pair separation of  $55''$ . This effect is partially mitigated by the tiling method (Blanton et al. 2003), which overlaps spectroscopic plates in order to yield full sky coverage. In plate overlap regions, galaxy pairs closer than  $55''$  can be recovered. However, this still leaves  $\sim 9\%$  of galaxies without measured redshifts (J11) and this can strongly affect clustering measurements on very small scales. Following the approach described in Masjedi et al. (2006, 2008), J11 used a cross-correlation technique between the imaging and spectroscopic samples to correct for fiber collisions and obtain unbiased  $w_p(r_p)$  measurements down to the  $10h^{-1}\text{kpc}$  scale. Details of the method can be found in §3 of J11.

A second potential problem that affects very small scales is that galaxies may be overlapping and the light within this region needs to be properly distributed between the two galaxies. This is known as “deblending”. M06 found a systematic error in the SDSS pipeline wherein too much light was allocated to the dimmer of the two galaxies. As a result, a galaxy that may have been too dim to make the LRG brightness cut could now be included in the sample. This increased the number of small-scale pairs and boosted the correlation function on very small scales. M06 quantified this effect and corrected their measurements accordingly. Since the physical sizes of galaxies decrease rapidly with decreasing luminosity, this photometric deblending error diminishes in lower luminosity samples. For this reason, J11 ignored this effect in the luminosity samples they considered ( $M_r < -18$  through  $-21$ ). Nevertheless, we estimate the maximum effect of deblending by applying the M06 LRG correction to the  $M_r < -21$  sample and repeating our analysis. We find that our results do not change qualitatively.

We restrict ourselves to modeling the J11 data points from  $\sim 10 - 400h^{-1}\text{kpc}$ . These can be seen in Figure 1, which shows  $w_p(r_p)$  scaled by an  $r_p^{-1}$  power law, with each panel corresponding to a distinct luminosity

threshold. The bottom right panel of Figure 1 shows the LRG data points measured by M06 and modeled by W10. Along with these 9 data points used in our modeling, we also incorporate the measured number density for each luminosity sample (see Table 1), providing a tenth data point. We use the full covariance matrices from the 9 J11  $w_p(r_p)$  data points for each sample, which were estimated using jackknife resampling of 50 regions on the sky. The same jackknife samples were used to estimate the error on each calculated number density.

## 3. REVIEW OF THE METHOD

### 3.1. The HOD and the Galaxy 2PCF

Here we briefly review the method used in W10, which is based on the halo occupation distribution (HOD) formalism. The HOD fully characterizes the number, velocity and spatial distribution of galaxies within dark matter halos. The probability distribution that a virialized dark matter halo of mass  $M$  will host  $N$  galaxies is designated as  $P(N|M)$ .  $\langle N \rangle_M$  is the first moment of  $P(N|M)$ , and is the mean number of galaxies as a function of halo mass. Motivated by theory (e.g., Berlind et al. 2003; Kravtsov et al. 2004; Zheng et al. 2005), we consider central galaxies that live at the center of their host halo and satellite galaxies that orbit within the host potential as separate terms. We thus write the first moment of the HOD as  $\langle N \rangle_M = 1 + \langle N_{\text{sat}} \rangle_M$ . Furthermore, we assume that there is some minimum halo mass,  $M_{\text{min}}$ , below which a halo will contain no galaxies and above which there will always be at least one central galaxy. For the satellite component, we adopt the parametric form,  $\langle N_{\text{sat}} \rangle_M = \exp[-M_0/(M_{\text{halo}} - M_{\text{min}})] \times (M_{\text{halo}}/M_1)^\alpha$ , where the satellite galaxies obey a power-law function of slope  $\alpha$  with an exponential cut-off at the low mass end at  $M_0$ .  $M_1$  is the characteristic mass scale where a halo will contain, on average, one central and one satellite galaxy.

To calculate the mean number of satellite galaxy pairs  $\langle N_{\text{sat}}(N_{\text{sat}} - 1) \rangle$  (the second moment of the satellite  $P(N|M)$ ), we assume that the number of satellite galaxies in a halo of mass  $M$  follows a Poisson distribution of mean  $\langle N_{\text{sat}} \rangle_M$ . This sort of HOD parameterization is widely used to model galaxy clustering data (Zehavi et al. 2005a,b, 2010; Tinker et al. 2005; Conroy et al. 2006; Zheng et al. 2007, 2009; Watson et al. 2011).

To characterize the spatial distribution of galaxies within their host halos, we initially take the approach of placing one galaxy at the center and assuming that satellites trace the underlying dark matter density distribution. The dark matter density profiles are described by the NFW relation  $\rho(r) \propto (c \frac{r}{R_{\text{vir}}})^{-1} (1 + c \frac{r}{R_{\text{vir}}})^{-2}$  (Navarro et al. 1997), where  $c$  is the concentration parameter,  $c \equiv R_{\text{vir}}/r_s$ , and  $r_s$  is the characteristic scale radius. We use the virial definition of a halo to calculate the virial radius of host halos, such that  $R_{\text{vir}} = ((3M)/(4\pi\Delta_{\text{vir}}\bar{\rho}))^{1/3}$ , where  $\Delta_{\text{vir}}$  is the mean halo overdensity ( $\Delta_{\text{vir}} = 200$ ), and  $\bar{\rho}$  is the mean density of the universe. The concentration - mass relation is given by Zheng et al. (2007) for the modification of Bullock et al. (2001):  $c = \frac{c_0}{(1+z)} \times (\frac{M_{\text{halo}}}{M_*})^{-\beta}$ , where  $c_0 = 11$ ,  $M_*$  is the non-linear collapse mass at the median redshift of the sample for our choice of cosmology ( $M_*$  is redshift de-

TABLE 1  
INPUT DATA FOR ALL LUMINOSITY SAMPLES

| $M_r$ | $\bar{n}_g$   | $z_{med}$ | $\log(M_*)$ |
|-------|---------------|-----------|-------------|
| -18.0 | 3.209 (0.169) | 0.032     | 12.4228     |
| -18.5 | 2.405 (0.131) | 0.039     | 12.4147     |
| -19.0 | 1.689 (0.092) | 0.046     | 12.4057     |
| -19.5 | 1.326 (0.058) | 0.059     | 12.3887     |
| -20.0 | 0.749 (0.018) | 0.078     | 12.3647     |
| -20.5 | 0.377 (0.009) | 0.097     | 12.3397     |
| -21.0 | 0.123 (0.002) | 0.116     | 12.3057     |

NOTE. —  $\bar{n}_g$  is measured in units of  $10^{-2}h^3\text{Mpc}^{-3}$  and the associated error from 50 jackknife samples on the sky is shown in parentheses.  $z_{med}$  is the median redshift as measured in J11.  $M_*$  is the non-linear collapse mass and is in units of  $h^{-1}M_\odot$ .

pendent and is thus uniquely defined for each luminosity sample and is given in Table 1) and  $\beta = 0.13$ .

The mean number density of galaxies can be calculated for a given HOD by weighting the abundance of halos by  $\langle N \rangle_M$  and integrating over all halo mass (see Eq.[2] of W10). We adopt the Warren et al. (2006) halo mass function,  $dn/dM$ , in all of our calculations, but our results are not sensitive to the specific choice of mass function.

To model the galaxy two-point correlation function (2PCF),  $\xi_{gg}$ , we use the halo model.  $\xi_{gg}$  can be decomposed into contributions due to galaxies residing in the same halo (the “one-halo” term) as well as galaxies living in separate, distinct halos (the “two-halo” term). Therefore,  $\xi_{gg}$  can be written as the sum of the one-halo and two-halo terms (e.g., Cooray & Sheth 2002; for this particular form of the equation see Zheng 2004):  $\xi_{gg}(r) = \xi_{gg}^{1\text{halo}} + \xi_{gg}^{2\text{halo}} + 1$ . Since we are probing such small scales we need only consider the one-halo term for modeling the correlation function. The one-halo term depends on the second moment of  $P(N|M)$ , as well as the pair separation distributions of central-satellite and satellite-satellite pairs (see Eq.[4] of W10 for the particular form). The pair separation distribution for central-satellite pairs is essentially the same as the density profile of satellite galaxies. The satellite-satellite pair distribution is the convolution of the density profile with itself and, as in W10, we use the Sheth et al. (2001) calculation for the convolution of a truncated NFW profile with itself. Therefore, we can start to see the link between the shape of  $\xi(r)$  and the shape of the satellite profile on small scales. This is discussed in detail in §4.

For each luminosity threshold, J11 measured the *projected* correlation function, so we convert our theoretical real-space correlation function  $\xi(r)$  to  $w_p(r_p)$  (Eq.[5] of W10). At each luminosity threshold, we integrate up to the  $\pi_{\text{max}}$  value given in Zehavi et al. (2010), which ranges from  $40 - 60h^{-1}\text{Mpc}$ . The method of J11 results in a  $\pi_{\text{max}}$  that is effectively larger than our choice. However, the difference is insignificant at the small scales we model. Integrating out to large scales means that the two-halo term cannot be entirely ignored. Since calculating the two-halo term correctly is fairly complex and its contribution to  $w_p(r_p)$  is minimal at the scales of the data points that we model, we use a simple approximation instead. We first calculate the large-scale bias of

galaxies,  $b_g$ ,

$$b_g = \bar{n}_g^{-1} \int_{M_{\min}}^{\infty} dM \frac{dn}{dM} b_h(M) \langle N \rangle_M, \quad (1)$$

where  $b_h(M)$  is the large-scale bias of halos. The two-halo term has a simple relation to the matter-matter correlation function on large scales:  $\xi_{gg}^{2\text{halo}} = b_g^2 \xi_{mm}$ . We consider the best-fit two-halo term from Zehavi et al. (2010) for each luminosity and append a newly defined two-halo term to our model one-halo term,

$$\xi_{gg}^{2\text{halo}} = \left( \frac{b_g}{b'_g} \right)^2 \xi_{gg}^{2\text{halo}'}, \quad (2)$$

where primes designate the Zehavi et al. (2010) values. In effect, we allow the amplitude of the 2-halo term to vary with HOD parameters, but we keep its shape fixed. The error introduced by this approximation is completely negligible as we have checked that a 20% shift in the amplitude of the two-halo term has no appreciable effect on  $w_p(r_p)$  at the maximum pair separation that we consider ( $0.4h^{-1}\text{Mpc}$ ) for any of the luminosity threshold samples. This test also emphasizes our insensitivity to the difference between our choice of integrating out to the  $\pi_{\text{max}}$  given by Zehavi et al. (2010) and the technique used by J11.

### 3.2. The PNM and PNMCG Models

W10 considered 4 distinct models for modeling the small-scale  $w_p(r_p)$  of LRGs. In this paper we need only consider two of the models, defined as:

- **PNM** - in this model the only free parameters are those associated with the  $P(N|M)$  distribution as described in §3.1 -  $M_{\min}$ ,  $M_0$ ,  $M_1$ , and  $\alpha$ . While these parameters are free to take on any value, the spatial distribution of satellite galaxies within halos is fixed to an NFW dark matter density profile. Since there are 10 data points (9 from the J11  $w_p(r_p)$  measurements along with the measured number density for each luminosity sample) and 4 free parameters, the PNM model has 6 degrees of freedom.
- **PNMCG** - this model allows for the same free parameters as the PNM model, with the exception of  $M_0$ .  $M_0$  was unconstrained in our initial MCMC runs (this was also the case in W10), thus we fixed  $M_0$  to  $M_{\min}$  throughout our analysis. The PNMCG model also considers a parametrized density profile for satellite galaxies. As in W10, we allow both the concentration and the inner slope of the density profile to be free. The satellite galaxy concentration can differ from the dark matter concentration (defined in §3.1) through the free parameter  $f_{\text{gal}}$ ,

$$c_{\text{gal}} = f_{\text{gal}} \times c. \quad (3)$$

The inner slope of the density profile is no longer fixed to -1, as is the case for an NFW profile, but rather is specified by the free parameter  $\gamma$ . As in W10, we adopt the following density profile for satellite galaxies

$$\rho(r) = \frac{\rho_s}{\left( c_{\text{gal}} \frac{r}{R_{\text{vir}}} \right)^\gamma \left( 1 + c_{\text{gal}} \frac{r}{R_{\text{vir}}} \right)^{3-\gamma}}. \quad (4)$$

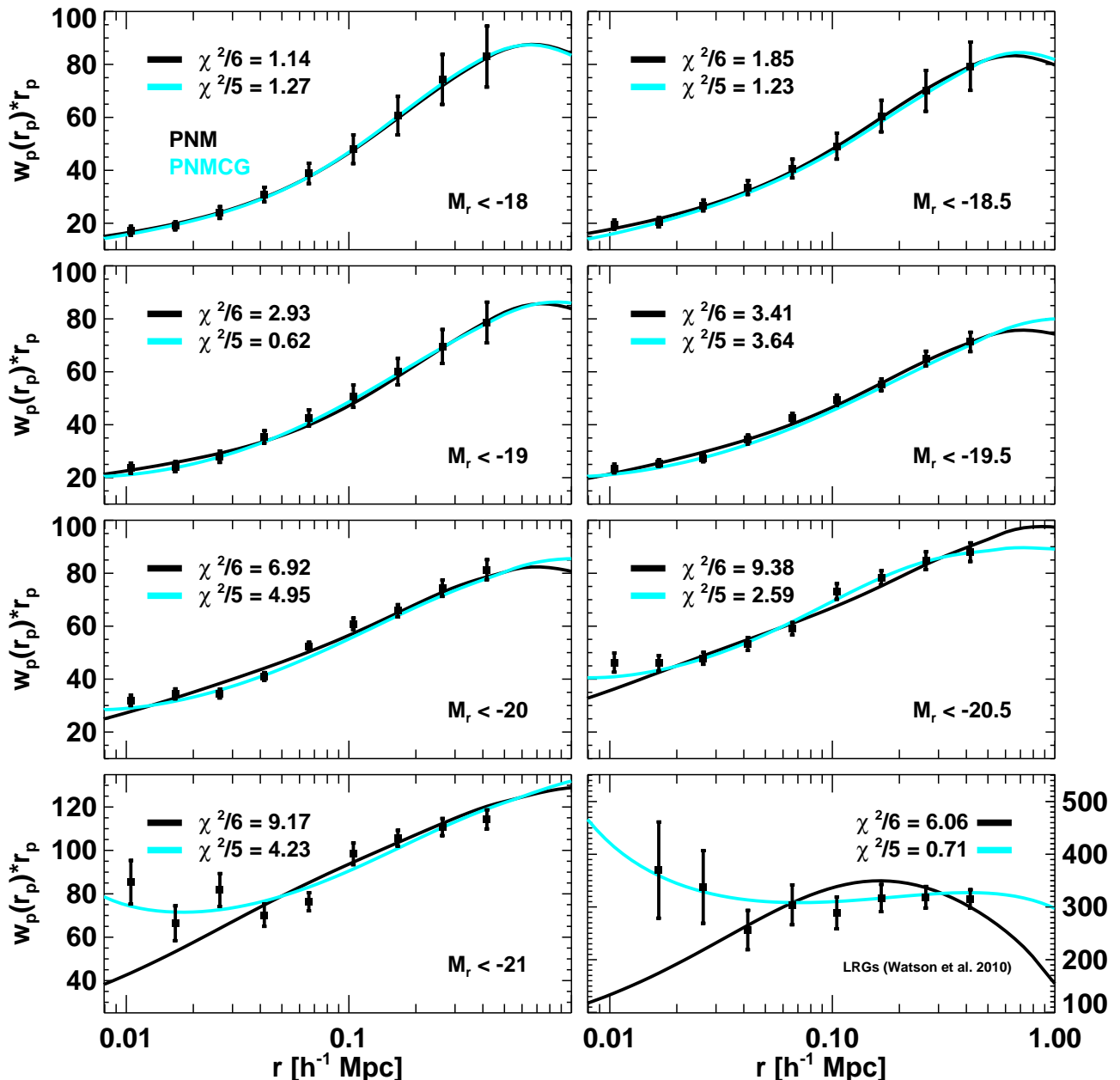


FIG. 1.— Model fits to the projected correlation function for luminosity thresholds spanning  $M_r < -18$  to LRGs. The points in the  $M_r < -18$  through  $M_r < -21$  panels show the Jiang et al. (2011)  $w_p(r_p)$  measurements (multiplied by  $r_p$ ) and their associated jackknife errors. The bottom right panel shows results for LRGs from Watson et al. (2010). The black curves show the best-fit PNM models, which use four-free parameters describing the probability distribution  $P(N|M)$  ( $M_{\min}$ ,  $M_1$ ,  $M_0$ , and  $\alpha$ ). The PNMCG model, shown in cyan, considers two additional free parameters (but  $M_0$  is fixed to  $M_{\min}$ ): (1)  $f_{\text{gal}}$ , which relates the concentration of the density profile of satellite galaxies relative to dark matter ( $f_{\text{gal}} = c_{\text{gal}}/c$ ), and (2)  $\gamma$ , which allows for the inner slope of the density profile to differ from the dark matter distribution. The reduced  $\chi^2$  values for each best-fit model are listed in each panel.

For an NFW profile  $\gamma = 1$ , however, the PNMCG model allows  $\gamma$  to take on any value from 0–4. This model considers the same number of data points as the PNM model, but now there are 5 free parameters ( $M_{\min}$ ,  $M_1$ ,  $\alpha$ ,  $f_{\text{gal}}$  and  $\gamma$ ) resulting in 5 degrees of freedom.

As detailed in §3.4 of W10, we use a Markov Chain Monte Carlo (MCMC) method to probe the parameter space for a given set of parameters (see Dunkley et al.

2005 for details on MCMC techniques). When a chain has converged, we can find the most likely value for each parameter by calculating the mean of its distribution. Errors for each parameter are given by the extrema of the middle 68.3% of the distribution. Best-fit parameters are found by the combination of parameter values for which  $\chi^2$  is a minimum.

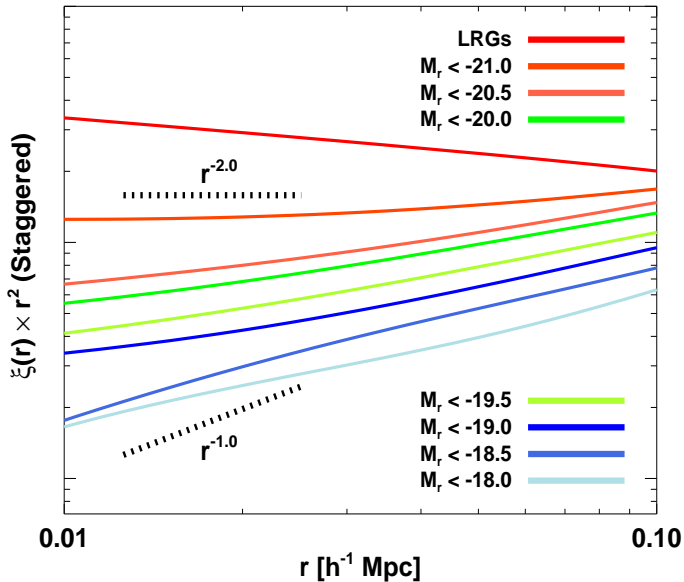


FIG. 2.— The real-space correlation function  $\xi(r)$  residuals from an  $r^{-2}$  power law from the PNMCG best-fit models before converting to the projected correlation functions of Fig. 1. Amplitudes have been arbitrarily shifted for clarity. The slope of  $\xi(r)$  on small scales is a reflection of the central-satellite pair distribution, which is essentially just the density profile itself. There is a strong luminosity dependence of the slope of  $\xi(r)$  on small scales, becoming steeper and steeper for the brighter galaxy samples and this carries directly over to the luminosity dependence of the radial profile of satellite galaxies. The dotted lines show  $r^{-1}$  and  $r^{-2}$  power-law slopes.

J11 measured  $w_p(r_p)$  to very small scales over a large range in luminosity thresholds. Their measurements nicely overlap those of Zehavi et al. (2010) on intermediate scales ( $\sim 0.2 - 7h^{-1}\text{Mpc}$ , see Fig. 14 in J11), and extend down to very small scales with the innermost data point for each sample at  $\sim 10h^{-1}\text{kpc}$ . As discussed in §3.2, for each luminosity threshold sample, we model  $w_p(r_p)$  with, (1) the PNM model, which only varies parameters that determine the number of galaxies in a given halo, but forces the satellite galaxies to have an NFW spatial distribution within their halo, and (2) the PNMCG model, which also allows the spatial distribution of satellite galaxies to vary within halos.

Figure 1 shows our modeling results for each luminosity sample.  $w_p(r_p)$  has been scaled by an  $r_p^{-1}$  power law to more clearly highlight any discrepancies between the PNM and PNMCG models. Each panel shows the SDSS data points as well as the best-fit model for the PNM (black curve) and PNMCG (cyan curve) cases. It is clear from the figure that as we go to higher luminosities, the PNMCG model provides a significantly better fit to the data. We find that the  $P(N|M)$  parameter distributions are nearly the same for the two models, differing by, at most,  $\sim 3\sigma$ . Therefore, the improved fits for the PNMCG model principally arise from the freedom to vary the density profile of satellite galaxies. Varying the density profile is thus necessary to find a better fit to the data as we go to higher luminosities.

We note that the reduced  $\chi^2$  values (listed in each panel) are in many cases quite high, even in the PNMCG case. This could mean that the PNMCG model

contains incorrect assumptions or does not have enough freedom. On the other hand, it could mean that the J11 jackknife errors are underestimated. To check the impact of the error estimates on our modeling, we re-estimated errors for the  $M_r < -20$  sample using mock galaxy catalogs from the LasDamas project (McBride et al. in prep.). We used 160 catalogs<sup>1</sup> and measured the dispersion of  $w_p(r_p)$  between the catalogs, using the same binning method as J11. We then applied the fractional error (with respect to the mean of all mock measurements) to the data (non-mock) measurement to estimate the absolute errors and full covariance. Finally, using our new mock based error estimates, we re-ran the MCMC chains for the PNMCG model. We then compared the best-fit parameter values for the two fits and found that the parameters did not change significantly. By this, we mean the difference in  $\chi^2$  between the two best-fit points were within  $1\sigma$  when evaluated with either of the likelihood surfaces (from each of the two MCMC runs with different errors). We conclude two things from this test: (1) our somewhat high  $\chi^2$  values are not overly concerning, and are likely due to a slight underestimate of the errors from jackknife re-sampling on the data, and (2) this issue does not seem to affect any of our conclusions.

We now investigate the luminosity dependence of the radial distribution of satellite galaxies and the degree to which it differs from an NFW distribution. As discussed in §3.1, when constructing the real-space correlation function in the halo model, the one-halo term considers contributions from central-satellite and satellite-satellite pairs. The central-satellite contribution, which is essentially just the density profile itself (see Eq. 4 of W10), is steeper than the satellite-satellite pair contribution and thus dominates the correlation function on the very small scales that we are considering (e.g., Figure 4. of Zheng et al. 2009). Therefore, the luminosity dependence of the *slope of  $\xi(r)$  on small scales* can give a direct indication of the luminosity dependence of the *radial profile of satellite galaxies*. Figure 2 shows the residuals from an  $r^{-2}$  power law from the PNMCG best-fit models shown in Figure 1. The amplitudes of the curves have been arbitrarily staggered simply to make the plot more clear. The dotted lines highlight the cases of  $r^{-1}$  and  $r^{-2}$  power laws. The slope of  $\xi(r)$  is clearly a strong function of luminosity, being close to -1 for low luminosity galaxies and going more and more towards -2 for the  $M_r < -21$  sample and even steeper for LRGs. The W10 result for the steepness of the slope of  $\xi(r)$  for LRGs on small scales was also found by Almeida et al. (2008). Using the Bower et al. (2006) semi-analytic model applied to the Millenium simulation (Springel et al. 2005), they found that the LRG real-space correlation function follows an  $\sim r^{-2.07}$  power law shape down to the  $\sim 10h^{-1}\text{kpc}$  scale.

We next wish to directly investigate the radial profiles of satellite galaxies that are required by the data and compare them to the NFW profile. For each luminosity sample, we choose a halo mass equal to the mean value of  $M_1$  in the PNMCG MCMC chain for that sample. We choose  $M_1$  because it represents the typical size halo that

<sup>1</sup> North-only SDSS footprint from the LasDamas "gamma" data release.

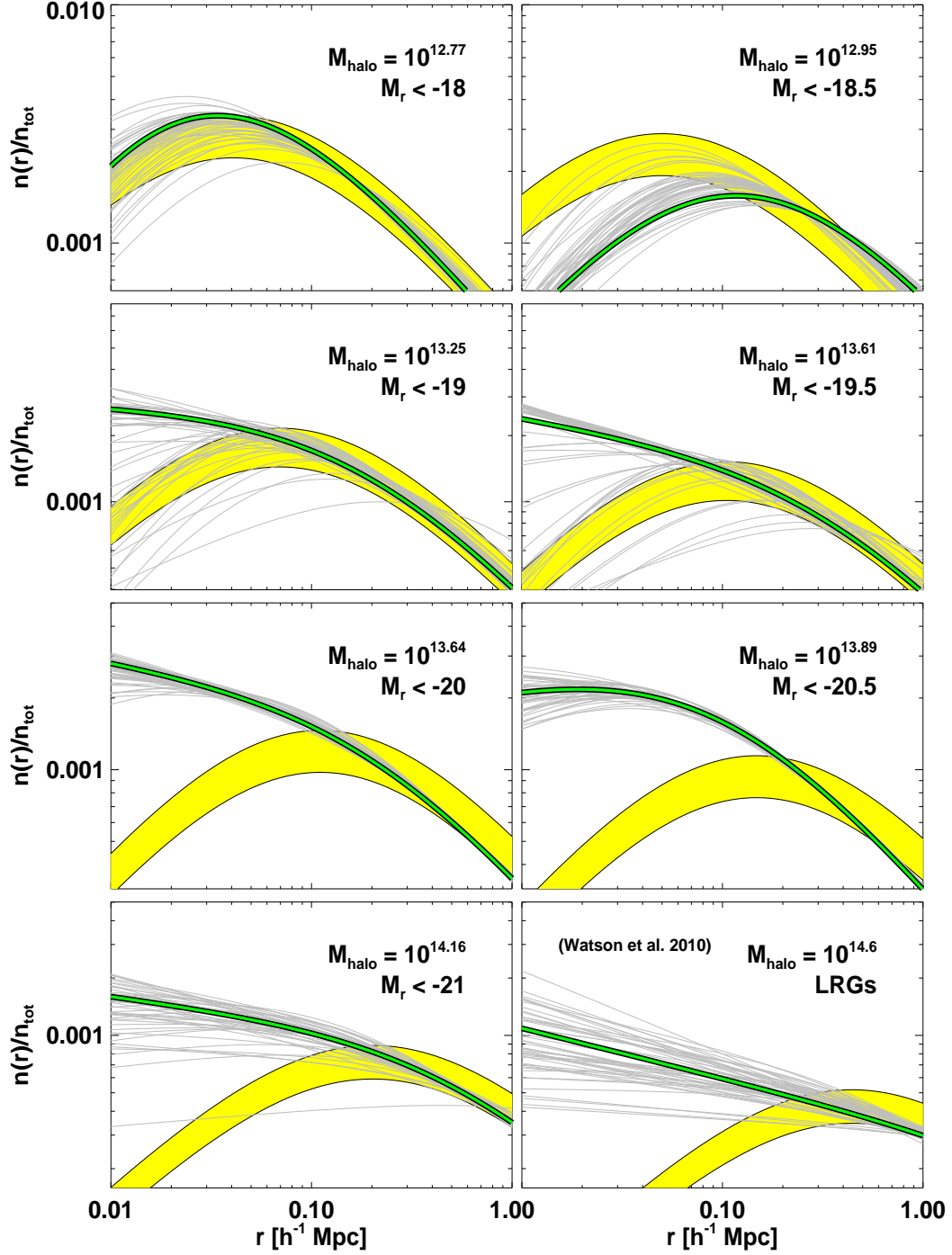


FIG. 3.— The radial profile of satellite galaxies as a function of luminosity. Each panel shows results for a specific luminosity sample, and for a halo mass that is chosen to be the mean value of  $M_1$  from the PNMCG MCMC chain (listed in the top right of the panel). The solid, yellow bands show the NFW profile, with a 20% uncertainty to account for the possible ambiguity in the dark matter distribution. Green curves show the profile corresponding to the best-fit PNMCG model. Each panel also contains 50 grey curves representing 50 randomly drawn links from the top 95% of the PNMCG MCMC chain, after sorting in  $\chi^2$  from lowest to highest values. These 50 curves thus span the 95% confidence region allowed by the data. As we probe higher luminosities, the radial profile of satellite galaxies strongly deviates from an NFW distribution on small scales, showing that luminous galaxies are poor tracers of the underlying dark matter.

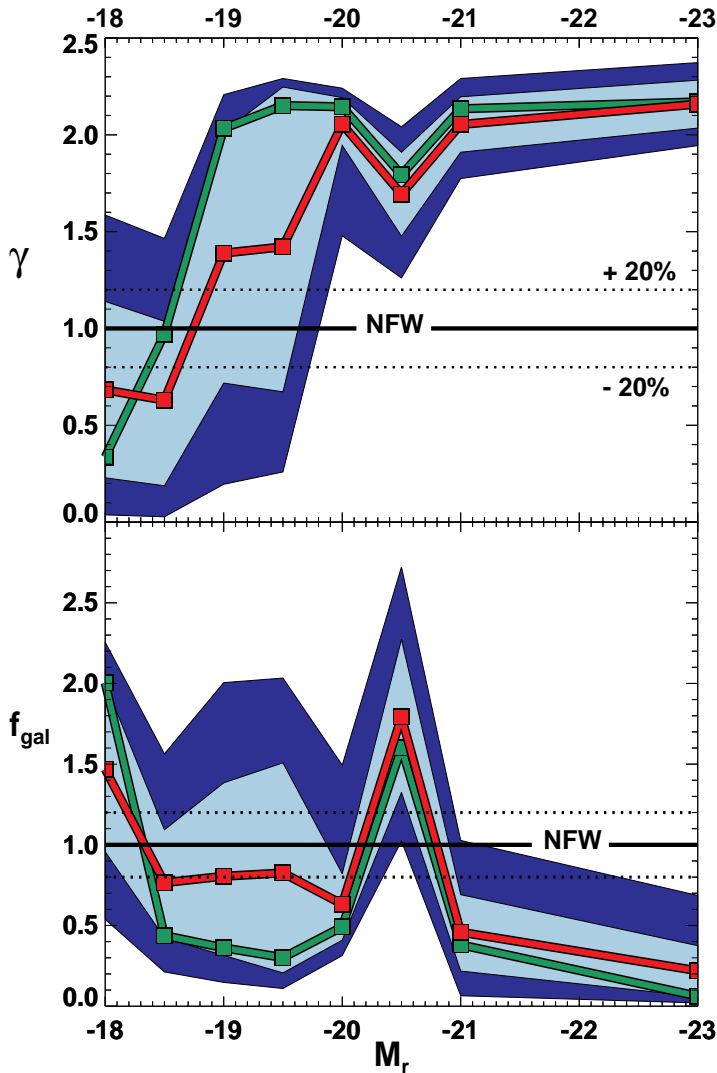


FIG. 4.— *Top Panel*: The slope of the inner density profile of satellite galaxies as a function of galaxy luminosity. The filled red squares (and connecting lines) show the mean value of  $\gamma$  from the MCMC chain of the PNMCG model for each luminosity sample and the green squares represent the best fit. The light blue and dark blue bands are the associated errors from the extrema of the middle 68.3% and 95% of the distribution, respectively.  $\gamma = 1$  corresponds to an inner slope for an NFW dark matter profile, and is shown as a solid black line. The dotted black lines highlight an assumed 20% inaccuracy in the dark matter profile. *Bottom Panel*: The same procedure as the top panel, but for the parameter  $f_{\text{gal}}$  which relates the galaxy and dark matter concentrations ( $f_{\text{gal}} = c_{\text{gal}}/c$ ).  $f_{\text{gal}}$  and  $\gamma$  are intrinsically linked and there is a strong trend towards inner slopes becoming steeper than NFW as we go to higher luminosities, with corresponding decreasing values of  $f_{\text{gal}}$ .

contributes central-satellite pairs to  $\xi(r)$  (smaller halos have no satellites and larger halos are rare). Specifying the halo mass sets the amplitude, virial radius, and dark matter concentration in Equation 4. The radial profile then only depends on the parameters  $f_{\text{gal}}$  and  $\gamma$ . We then take the full MCMC chain for the PNMCG model and sort it by  $\chi^2$  from lowest to highest. We then randomly draw 50 links from the top 95% of the chain. Each of these links has distinct values of  $f_{\text{gal}}$  and  $\gamma$ , which we insert into Equation 4 in order to construct individual radial profiles. The light grey curves in each panel of

Figure 3 show these 50 profiles (multiplied by  $4\pi r^2 dr$  to convert them from density into mass profiles). These curves thus span the 95% confidence region allowed by the data. The green curve in each panel shows the radial profile corresponding to the best-fit PNMCG model. To compare with the NFW profile for dark matter, we also plot the case  $f_{\text{gal}} = 1$ ,  $\gamma = 1$ , shown by the yellow bands. We assume that the dark matter profile of halos has a 20% uncertainty, which we represent as the thickness of the bands (see §5 for discussion of the uncertainties in the dark matter distribution in halos). Figure 3 shows, once again, that galaxies of increasing luminosity deviate more from an NFW profile. In fact, the figure seems to suggest that there is a transition point, somewhere between an absolute  $r$ -band magnitude of  $-19.5$  and  $-20$ , where the radial profile of satellite galaxies goes from being consistent with NFW to completely inconsistent. For the highest luminosity samples, the profiles approach a power-law shape.

Figure 4 shows the luminosity dependence of the inner slope and concentration of satellite galaxies as found by the PNMCG model. The dark blue and light blue bands in each panel represent the middle 95% and 68.3% of the MCMC chains after first sorting in  $\gamma$  (top panel) and sorting in  $f_{\text{gal}}$  (bottom panel). The filled red squares show the mean of the respective parameters in the MCMC chain for each luminosity sample and filled green squares show the best-fit values. The solid black line highlights the NFW dark matter inner slope of the density profile which corresponds to  $\gamma = f_{\text{gal}} = 1$  and the dotted lines represent the possible 20% ambiguity of an assumed NFW inner slope and concentration. The  $M_r < -18, -18.5, -19$  and  $-19.5$  samples have large spreads in  $\gamma$  and  $f_{\text{gal}}$  values, as there are many parameter combinations that can yield a similar goodness-of-fit to the data. For  $M_r < -20$  and brighter galaxies, both  $\gamma$  and  $f_{\text{gal}}$  have tighter distributions and deviate from NFW. Figure 4 shows that there is a strong luminosity dependence of the satellite galaxy profile, i.e.  $\gamma$  is an increasing function of luminosity, and  $f_{\text{gal}}$  is a decreasing one. However, notice the unique coupling of  $f_{\text{gal}}$  and  $\gamma$  for the  $-20.5$  case, where  $f_{\text{gal}}$  seems to deviate from the aforementioned trend.  $\gamma$  for  $-20.5$  satellite galaxies also strays from the trend, but it is still significantly larger than NFW. For  $M_r < -20$  and brighter galaxies, the mean value of  $\gamma$  ranges between 1.6 - 2.1, significantly steeper than NFW. This range of  $\gamma$  values persists all the way down to  $M_r < -19$  when considering the best-fit values. As mentioned in §2, M06 found a systematic error in the manner that light in the overlapping region of LRG pairs was being allocated in the SDSS pipeline. This caused a slight boost in the small-scale correlation function and was corrected for by M06. This effect is expected to rapidly diminish for lower luminosity samples, because the intrinsic sizes of galaxies will be smaller. However, we apply the same LRG correction to the J11  $M_r < -21$  sample to model the maximum effect that this could have. While we expect  $\langle \gamma \rangle$  to decrease as a result of the innermost data points being scaled to lower  $w_p(r_p)$  values, we still find that  $\langle \gamma \rangle \sim 1.6$ . Thus, even after assuming a *drastic* over-correction,  $\gamma$  is still strongly discrepant from NFW.

Figure 4 showed the luminosity trends for  $\gamma$  and  $f_{\text{gal}}$  by sorting the MCMC chains separately for each param-

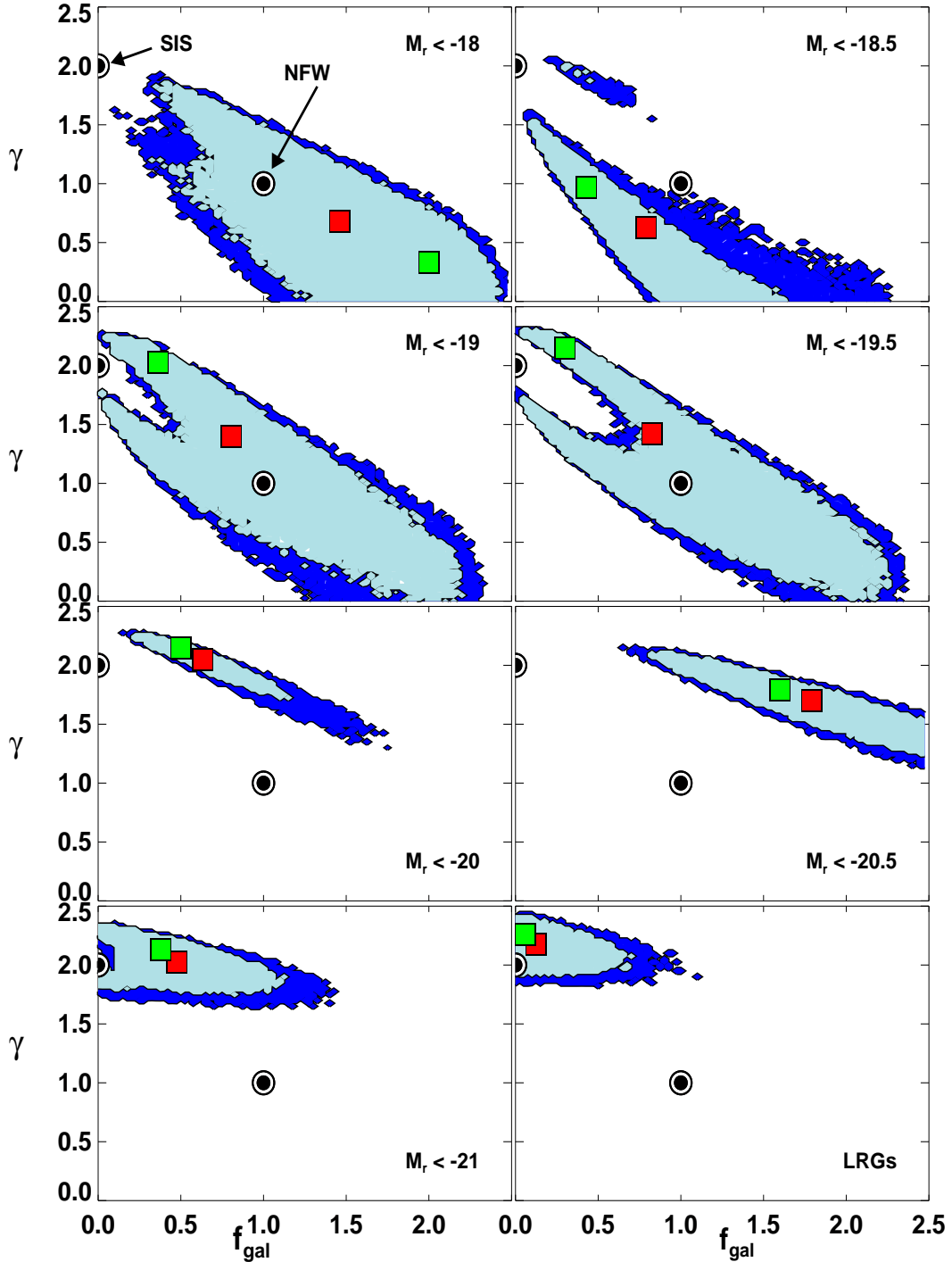


FIG. 5.— The  $\gamma$ – $f_{\text{gal}}$  parameter space as a function of luminosity, highlighting the relationship between the inner slope and concentration of the density profile of satellite galaxies relative to dark matter. For each panel, the dark blue and light blue regions are defined as the top 95% and 68.3% of the MCMC chain for a given luminosity sample after sorting in  $\chi^2$ . There are two points of reference designated as filled circles - the  $\gamma = 1, f_{\text{gal}} = 1$  combination that represents an NFW distribution, and the  $\gamma = 2, f_{\text{gal}} \rightarrow 0$  combination that represents a singular isothermal sphere distribution (SIS). Red squares show the mean values of  $\gamma$  and  $f_{\text{gal}}$  from our MCMC runs and green squares show the values for the best-fit model. The data for  $M_r < -20$  and brighter galaxies strongly rule out the NFW model and are in good agreement with an SIS distribution for  $M_r < -21$  and LRGs.

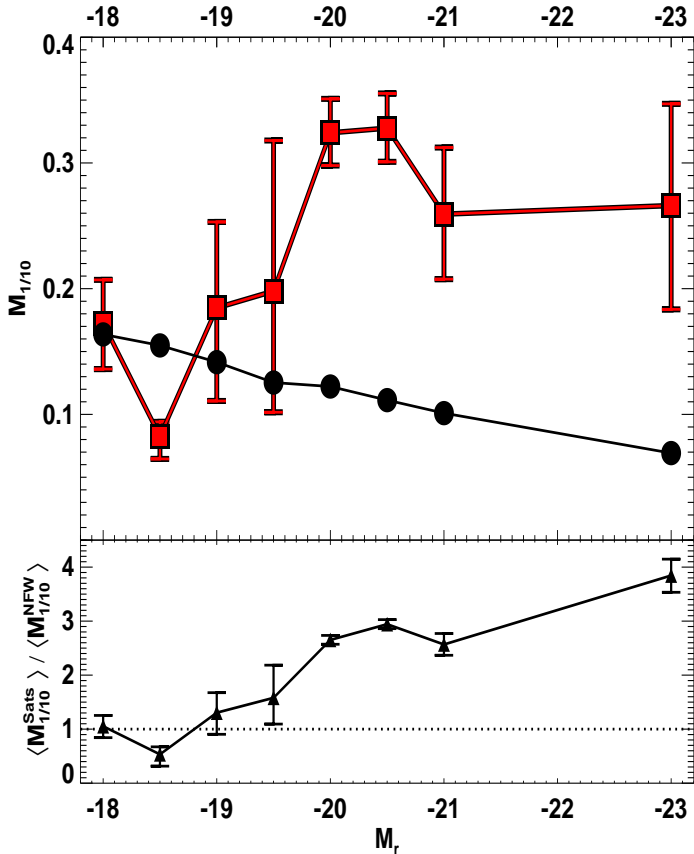


FIG. 6.— A more physically useful definition of concentration:  $M_{1/10}$ , defined as the fraction of satellite galaxies (or mass) that are enclosed within one tenth of the virial radius of a halo (see Eq. 5). *Top Panel:* For each luminosity sample, we choose a mass equal to the mean value of  $M_1$  from the PNMCG MCMC chain, and we compute  $M_{1/10}$  for each link in the chain. Red squares (and connecting lines) show the mean of the  $M_{1/10}$  distribution for a given luminosity, and errorbars for  $M_{1/10}$  show the extrema of the middle 68.3% of the distribution. Black points show  $M_{1/10}$  for an NFW distribution. *Bottom Panel:* Ratio of  $M_{1/10}$  for satellites with respect to dark matter. The dotted line highlights a ratio of unity. Satellite galaxies clearly become much more centrally concentrated than dark matter with increasing luminosity.

eter. However,  $\gamma$  and  $f_{\text{gal}}$  are intrinsically coupled to one another so it is important to investigate the joint  $\gamma - f_{\text{gal}}$  parameter space. Figure 5 Shows the  $\gamma - f_{\text{gal}}$  parameter space at each luminosity, with the dark blue and light blue regions defined as the top 95% and 68.3% of the MCMC chain, after sorting in  $\chi^2$ . There are two points of reference designated as filled circles: the  $\gamma = 1, f_{\text{gal}} = 1$  combination for an NFW distribution and a  $\gamma = 2, f_{\text{gal}} \rightarrow 0$  combination representing a singular isothermal sphere (SIS) distribution. Red squares represent the mean values of  $\gamma$  and  $f_{\text{gal}}$  from our MCMC runs and green squares show the best-fit combination. As expected, the  $M_r < -18$  through  $-19.5$  exhibit a broad range in  $\gamma - f_{\text{gal}}$  combinations, with the NFW combination lying within the top 68.3% region (with the exception of the  $-18.5$  sample). The  $\gamma - f_{\text{gal}}$  regions clearly drift away from NFW for  $M_r < -20$  and greater luminosities and are well described by an SIS distribution for both the  $-21$  and LRG samples. Figure 5 shows that the

inner slope and concentration parameters are strongly degenerate with each other, particularly at low luminosities. This can be caused by having the scale radius (the radius within the halo where the slope transitions from  $-\gamma$  to  $-3$ ) too close to the innermost data point. When this happens, the data cannot accurately constrain the inner slope, and only constrains  $\gamma$  and  $f_{\text{gal}}$  through their degenerate contribution to the amplitude of the density profile. A simple calculation of the scale radius using the virial definition of a halo (see §3.1) gives  $r_s \sim 10h^{-1}\text{kpc}$  for the  $M_r < -18$  sample (adopting a halo mass equal to the mean value of  $M_1$ ), which is precisely at the scale of the innermost data point of  $w_p(r_p)$ . This leads to the large spread in  $\gamma - f_{\text{gal}}$  combinations. Of course, as we go to brighter samples, the scale radii increase, and the parameters are better constrained.

For each luminosity, as the inner profile steepens,  $f_{\text{gal}}$  decreases (with the slight deviation for the  $M_r < -20.5$  case). The decrease in concentration does not necessarily imply that the concentration of satellites is low in the traditional sense - i.e., that there are fewer galaxies at small radii - but rather that the radial profiles simply evolve toward a more power-law form. For example, as  $f_{\text{gal}} \rightarrow 0$  in the case of LRGs, this does not mean that the LRG satellites are less concentrated than the underlying dark matter. As  $f_{\text{gal}} \rightarrow 0$ , the scale radius is pushed far outside the virial radius, resulting in a pure power-law distribution of slope  $-\gamma$ . Since the value of  $f_{\text{gal}}$  can be misleading when thinking about the concentration of satellite galaxies, we consider an alternative definition of “concentration” that is more physically useful: the fraction of satellite galaxies (or mass) that are enclosed within a tenth of the virial radius  $R_{\text{vir}}$ . We call this quantity  $M_{1/10}$  and compute it by integrating any radial profile out to one-tenth the virial radius of the host halo and dividing by the total mass out to  $R_{\text{vir}}$

$$M_{1/10} = \frac{M(r < 0.1R_{\text{vir}})}{M(r < R_{\text{vir}})}. \quad (5)$$

Figure 6 (top panel) shows  $M_{1/10}$  as a function of luminosity. For each luminosity sample, we assume a halo mass equal to the mean value of  $M_1$  from the MCMC chain, and we calculate  $M_{1/10}$  for every link in the chain using each link’s values for  $\gamma$  and  $f_{\text{gal}}$ . We then find the mean of the distribution of  $M_{1/10}$  values (denoted by the red squares and connecting lines). Errors for  $M_{1/10}$  are given by the extrema of the middle 68.3% of the distribution. The black filled circles show  $M_{1/10}$  for a dark matter NFW profile. The dark matter concentration drops with luminosity because the mean value of  $M_1$  increases with luminosity and concentration is a decreasing function of halo mass (Bullock et al. 2001). The bottom panel of Figure 6 shows the ratio of  $M_{1/10}$  for satellites with respect to dark matter. The figure clearly shows that low luminosity satellite galaxies ( $M_r > -19.5$ ) have spatial concentrations similar to dark matter, whereas the profiles of luminous satellite galaxies ( $M_r < -20$  and brighter) are  $\sim 2.5 - 4$  times more concentrated than NFW.

## 5. SUMMARY & DISCUSSION

Do satellite galaxies trace the underlying dark matter distribution? Our modeling of the small-scale  $w_p(r_p)$  over an enormous range in galaxy luminosity thresholds,

from SDSS Main galaxies to LRGs ( $M_r < -18$  through  $\lesssim -23$ ), has revealed a strong luminosity dependence of the radial distribution of satellite galaxies. We have found that for the low luminosity samples (lower than  $M_r < -20$ ), there is a wide range of satellite galaxy concentrations (equal to  $f_{\text{gal}}$  times the NFW dark matter concentration) and inner density profile slopes,  $-\gamma$ , that are consistent with the data. This lack of constraining power is due to a strong degeneracy between  $f_{\text{gal}}$  and  $\gamma$ , which, in turn, is possibly due to the fact that the smallest scale data point in  $w_p(r_p)$  is roughly around the scale radius for halos hosting galaxies of this size. Nevertheless, low luminosity satellite galaxies have radial distributions that are generally consistent with the NFW dark matter distribution. When we move to higher luminosity galaxies ( $M_r < -20$  and brighter samples) however, satellite profiles change dramatically, with the most striking feature being that  $\gamma$  jumps to much higher values. Our results show that for  $M_r < -20$  and brighter galaxies,  $\gamma$  ranges from  $\sim 1.6 - 2.1$ , highly discrepant from NFW, even after assuming a 20% inaccuracy in the dark matter profile. Luminous satellite galaxies are thus poor tracers of the underlying dark matter within halos on the small scales that we probe. Since the effects of  $f_{\text{gal}}$  and  $\gamma$  on the radial profile are intertwined, we have calculated a more physically useful quantity  $M_{1/10}$ , which gives the fractional amount of mass enclosed within one-tenth of the virial radius. We find that  $M_{1/10}$  is a strong function of luminosity, being consistent with NFW for low luminosity galaxies and being  $\sim 2.5 - 4$  times more concentrated than NFW for galaxies brighter than  $M_r < -20$ .

What have previous studies found regarding the radial distribution of galaxies within halos? The concentration for satellite galaxies around isolated  $\sim L^*$  galaxies has been shown to be shallower than the dark matter concentration (Chen et al. 2006; Chen 2009). More et al. (2009) looked at faint satellites around bright central galaxies determined from SDSS satellite galaxy kinematics and, in this regime, the satellites exhibit a cored profile best described by a  $\gamma = 0, f_{\text{gal}} = 2$  combination. The concentration of subhalos in galaxy clusters has also been shown to be suppressed relative to the dark matter (Gao et al. 2004; Nagai & Kravtsov 2005). All of these results seem to go against what we find, though the masses and scales involved are not the same. We find that  $\sim L^*$  and brighter satellites within group and cluster sized halos have a steeper radial profile than dark matter on scales smaller than  $\sim 100h^{-1}\text{kpc}$ .

How do we interpret this result for luminous galaxies? Could NFW be a poor model for the dark matter distribution? In the established  $\Lambda\text{CDM}$  concordance cosmology, recent studies invoking high resolution N-body simulations have shown that the mass profiles of  $\Lambda\text{CDM}$  halos slightly, but systematically, deviate from NFW, becoming shallower at smaller radii (Stadel et al. 2009; Del Popolo 2010). In fact, they may be better described by Einasto profiles, which include a parameter  $\alpha$  that controls how the logarithmic slope will vary with radius to accurately account for the fact that halo profiles seem to not be self-similar (Gao et al. 2008; Navarro et al. 2010; Ludlow et al. 2010). These studies find, on average,  $\gamma < 1$  (Graham et al. 2006; Navarro et al. 2010). However, on average, the simpler, two-parameter NFW model, which has a characteristic  $r^{-1}$  inner slope, is ac-

curate to within 10 – 20% (Benson 2010). Moreover, Mandelbaum et al. (2008) fit galaxy cluster weak lensing profiles on small scales and found that NFW and Einasto profiles gave the same result to within several percent. Therefore, for simplicity, and to be consistent with previous modeling of LRGs by Watson et al. (2010), we assumed an NFW distribution throughout our modeling analysis. We conclude from the aforementioned studies that NFW is not a poor model for the dark matter distribution in collisionless simulations and, to the extent that it is, the true profile is even more discrepant from our results for luminous satellite galaxies.

Of course, by assuming a pure dark matter profile established from high resolution N-body simulations, the effects that baryons can have on dark matter are not considered. *Adiabatic Contraction* (AC) (Blumenthal et al. 1986; Ryden & Gunn 1987; Gnedin et al. 2004) may cause a steepening of the inner slope of the dark matter density profile as the gas condenses and sinks to the center of the dark matter potential well (Diemand et al. 2004; Fukushige et al. 2004; Reed et al. 2005; Del Popolo & Kroupa 2009). However, the majority of results indicate that the steepening is insubstantial or can vary widely from halo to halo (e.g., Tissera et al. 2010). In fact, while AC may cause a steepening of the inner profile, over time, major and minor mergers can cause the dark matter profile to become shallower. (El-Zant et al. 2001; Romano-Díaz et al. 2008, 2009; Johansson et al. 2009). Observational confirmations of AC are notoriously difficult. In the case of galaxy clusters, X-ray analysis by Zappacosta et al. (2006) showed that processes during halo formation (e.g. gravitational heating from merger events) counteract AC and the mass profiles were still well described by NFW. Mandelbaum et al. (2006) used galaxy-galaxy lensing to show that the mass density profile of LRG clusters is consistent with NFW. Recently, Schulz et al. (2010) studied the profiles of a large sample of SDSS ellipticals and found that their dynamical mass measurements suggest that the measured excess mass on small scales *may* be consistent with the AC hypothesis. However, for bright galaxies, our results are still not reconcilable with current AC models. We thus conclude that luminous satellite galaxies are indeed poor tracers of the underlying dark matter distribution, even accounting for the effects of baryons on the dark matter.

It is perhaps not surprising that galaxies do not behave like test particles as they orbit within a dark matter potential well. Being massive and extended, they are subject to dynamical mechanisms that would not affect test particles, namely dynamical friction and mass loss due to the tidal field of their host halo. In fact, these mechanisms should affect large and massive objects more than small ones, which could explain the luminosity trend that we observe. Satellite galaxies are thought to reside within subhalos, so it makes more sense to compare the radial distribution of galaxies to that of subhalos, rather than just dark matter. While subhalos tend to have a less concentrated radial distribution than dark matter (Ghigna et al. 1998, 2000; Gao et al. 2004; De Lucia et al. 2004; Nagai & Kravtsov 2005), the subhalo distribution has yet to be extended down to the extreme small scales that we have probed. High resolution N-body simulations are just now becoming avail-

able that allow for subhalos to be distinguished at the  $10h^{-1}\text{kpc}$  separation level (e.g., Klypin et al. 2010) for all of the luminosity samples that we have studied. Of course, subhalos may not be perfect tracers of galaxies, but it will be interesting to see whether the distribution of subhalos as a function of mass follows the same trend that we have uncovered for satellite galaxies as a function of luminosity. If the primary cause of this trend is dynamical in nature (e.g., dynamical friction), it should also show up with subhalos. Either way, such a comparison will yield insight into the relation between subhalos

and galaxies on very small scales, as well as the complicated non-linear processes occurring towards the centers of host halos, crucial for galaxy formation theory.

## 6. ACKNOWLEDGEMENTS

AAB is supported by Vanderbilt University and the Alfred P. Sloan Foundation. We thank Zheng Zheng for providing us with his best-fit 2-halo term for all the galaxy samples.

## REFERENCES

- Abazajian, K. N., et al. 2009, *ApJS*, 182, 543  
 Almeida, C., Baugh, C. M., Wake, D. A., Lacey, C. G., Benson, A. J., Bower, R. G., & Pimblet, K. 2008, *MNRAS*, 386, 2145  
 Benson, A. J. 2010, *Phys. Rep.*, 495, 33  
 Berlind, A. A., & Weinberg, D. H. 2002, *ApJ*, 575, 587  
 Berlind, A. A., et al. 2003, *ApJ*, 593, 1  
 Blanton, M. R., et al. 2003, *ApJ*, 594, 186  
 ——. 2005, *AJ*, 129, 2562  
 Blumenthal, G. R., Faber, S. M., Flores, R., & Primack, J. R. 1986, *ApJ*, 301, 27  
 Bower, R. G., Benson, A. J., Malbon, R., Helly, J. C., Frenk, C. S., Baugh, C. M., Cole, S., & Lacey, C. G. 2006, *MNRAS*, 370, 645  
 Bullock, J. S., Kolatt, T. S., Sigad, Y., Somerville, R. S., Kravtsov, A. V., Klypin, A. A., Primack, J. R., & Dekel, A. 2001, *MNRAS*, 321, 559  
 Chen, J. 2009, *A&A*, 494, 867  
 Chen, J., Kravtsov, A. V., Prada, F., Sheldon, E. S., Klypin, A. A., Blanton, M. R., Brinkmann, J., & Thakar, A. R. 2006, *ApJ*, 647, 86  
 Conroy, C., Wechsler, R. H., & Kravtsov, A. V. 2006, *ApJ*, 647, 201  
 Cooray, A., & Sheth, R. 2002, *Phys. Rep.*, 372, 1  
 De Lucia, G., Kauffmann, G., Springel, V., White, S. D. M., Lanzoni, B., Stoehr, F., Tormen, G., & Yoshida, N. 2004, *MNRAS*, 348, 333  
 Del Popolo, A. 2010, *MNRAS*, 408, 1808  
 Del Popolo, A., & Kroupa, P. 2009, *ArXiv e-prints*  
 Diemand, J., Moore, B., & Stadel, J. 2004, *MNRAS*, 353, 624  
 Dunkley, J., Bucher, M., Ferreira, P. G., Moodley, K., & Skordis, C. 2005, *MNRAS*, 356, 925  
 El-Zant, A., Shlosman, I., & Hoffman, Y. 2001, *ApJ*, 560, 636  
 Fukushige, T., Kawai, A., & Makino, J. 2004, *ApJ*, 606, 625  
 Gao, L., De Lucia, G., White, S. D. M., & Jenkins, A. 2004, *MNRAS*, 352, L1  
 Gao, L., Navarro, J. F., Cole, S., Frenk, C. S., White, S. D. M., Springel, V., Jenkins, A., & Neto, A. F. 2008, *MNRAS*, 387, 536  
 Ghigna, S., Moore, B., Governato, F., Lake, G., Quinn, T., & Stadel, J. 1998, *MNRAS*, 300, 146  
 ——. 2000, *ApJ*, 544, 616  
 Gnedin, O. Y., Kravtsov, A. V., Klypin, A. A., & Nagai, D. 2004, *ApJ*, 616, 16  
 Graham, A. W., Merritt, D., Moore, B., Diemand, J., & Terzić, B. 2006, *AJ*, 132, 2701  
 Jiang, T., Hogg, D. W., & Blanton, M. R. 2011, *In Preparation*.  
 Johansson, P. H., Naab, T., & Ostriker, J. P. 2009, *ApJ*, 697, L38  
 Klypin, A., Trujillo-Gomez, S., & Primack, J. 2010, *ArXiv e-prints*  
 Kravtsov, A. V., Berlind, A. A., Wechsler, R. H., Klypin, A. A., Gottlöber, S., Allgood, B., & Primack, J. R. 2004, *ApJ*, 609, 35  
 Ludlow, A. D., Navarro, J. F., Springel, V., Vogelsberger, M., Wang, J., White, S. D. M., Jenkins, A., & Frenk, C. S. 2010, *MNRAS*, 406, 137  
 Mandelbaum, R., Seljak, U., Cool, R. J., Blanton, M., Hirata, C. M., & Brinkmann, J. 2006, *MNRAS*, 372, 758  
 Mandelbaum, R., Seljak, U., & Hirata, C. M. 2008, *J. Cosmology Astroparticle Phys.*, 8, 6  
 Masjedi, M., Hogg, D. W., & Blanton, M. R. 2008, *ApJ*, 679, 260  
 Masjedi, M., et al. 2006, *ApJ*, 644, 54  
 More, S., van den Bosch, F. C., Cacciato, M., Mo, H. J., Yang, X., & Li, R. 2009, *MNRAS*, 392, 801  
 Nagai, D., & Kravtsov, A. V. 2005, *ApJ*, 618, 557  
 Navarro, J. F., Frenk, C. S., & White, S. D. M. 1997, *ApJ*, 490, 493  
 Navarro, J. F., et al. 2010, *MNRAS*, 402, 21  
 Peacock, J. A., & Smith, R. E. 2000, *MNRAS*, 318, 1144  
 Reed, D., Governato, F., Verde, L., Gardner, J., Quinn, T., Stadel, J., Merritt, D., & Lake, G. 2005, *MNRAS*, 357, 82  
 Romano-Díaz, E., Shlosman, I., Heller, C., & Hoffman, Y. 2009, *ApJ*, 702, 1250  
 Romano-Díaz, E., Shlosman, I., Hoffman, Y., & Heller, C. 2008, *ApJ*, 685, L105  
 Ryden, B. S., & Gunn, J. E. 1987, *ApJ*, 318, 15  
 Schulz, A. E., Mandelbaum, R., & Padmanabhan, N. 2010, *MNRAS*, 408, 1463  
 Scoccimarro, R., Sheth, R. K., Hui, L., & Jain, B. 2001, *ApJ*, 546, 20  
 Sheth, R. K., Diaferio, A., Hui, L., & Scoccimarro, R. 2001, *MNRAS*, 326, 463  
 Springel, V., et al. 2005, *Nature*, 435, 629  
 Stadel, J., Potter, D., Moore, B., Diemand, J., Madau, P., Zemp, M., Kuhlen, M., & Quilis, V. 2009, *MNRAS*, 398, L21  
 Strauss, M. A., et al. 2002, *AJ*, 124, 1810  
 Tinker, J. L., Weinberg, D. H., Zheng, Z., & Zehavi, I. 2005, *ApJ*, 631, 41  
 Tissera, P. B., White, S. D. M., Pedrosa, S., & Scannapieco, C. 2010, *MNRAS*, 406, 922  
 Warren, M. S., Abazajian, K., Holz, D. E., & Teodoro, L. 2006, *ApJ*, 646, 881  
 Watson, D. F., Berlind, A. A., McBride, C. K., & Masjedi, M. 2010, *ApJ*, 709, 115  
 Watson, D. F., Berlind, A. A., & Zentner, A. R. 2011, *ArXiv e-prints*  
 York, D. G., et al. 2000, *AJ*, 120, 1579  
 Zappacosta, L., Buote, D. A., Gastaldello, F., Humphrey, P. J., Bullock, J., Brighenti, F., & Mathews, W. 2006, *ApJ*, 650, 777  
 Zehavi, I., et al. 2005a, *ApJ*, 621, 22  
 ——. 2004, *ApJ*, 608, 16  
 ——. 2010, *ArXiv e-prints*  
 ——. 2005b, *ApJ*, 630, 1  
 Zheng, Z. 2004, *ApJ*, 610, 61  
 Zheng, Z., et al. 2005, *ApJ*, 633, 791  
 Zheng, Z., Coil, A. L., & Zehavi, I. 2007, *ApJ*, 667, 760  
 Zheng, Z., Zehavi, I., Eisenstein, D. J., Weinberg, D. H., & Jing, Y. P. 2009, *ApJ*, 707, 554